


# Beyond the Rozanov bound on electromagnetic absorption via periodic temporal modulations

Zeki Hayran<sup>1</sup> and Francesco Monticone<sup>1\*</sup>

*School of Electrical and Computer Engineering, Cornell University, Ithaca, New York 14853, USA*

 (Received 13 July 2023; revised 26 December 2023; accepted 21 February 2024; published 2 April 2024)

Incorporating time-varying elements into electromagnetic systems has been shown to be a powerful approach to challenge well-established performance limits, for example, bounds on absorption and impedance matching. So far, most of these studies have concentrated on time-switched systems, where the material undergoes instantaneous modulation in time while the input field is entirely contained within it. This approach, however, necessitates accurate timing of the switching event and limits how thin the system can ultimately be because of the spatial width of the impinging pulse. To address these challenges, here we investigate the *periodic* temporal modulation of highly lossy materials, focusing on their relatively unexplored parametric absorption aspects. Our results reveal that, by appropriate selection of the modulation parameters, the absorption performance of a periodically modulated absorber can be greatly improved compared with that of its time-invariant counterpart, and can even exceed the theoretical bound for conventional electromagnetic absorbers, namely, the “Rozanov bound.” Our findings thus demonstrate the potential of periodic temporal modulations to enable significant improvements in absorber performance while circumventing the limitations imposed by precise timing and material thickness in time-switched schemes, opening up new opportunities for the design and optimization of advanced electromagnetic absorber systems for various applications.

DOI: [10.1103/PhysRevApplied.21.044007](https://doi.org/10.1103/PhysRevApplied.21.044007)

## I. INTRODUCTION

Electromagnetic absorbers have become indispensable components in various applications across the electromagnetic spectrum, including energy harvesting, photovoltaics, sensing, radar-cross-section reduction, electromagnetic interference shielding, and stealth technologies. Over the years, a wide range of engineered absorber structures have been developed to fulfill diverse operational requirements, including Salisbury screens [1], Jaumann layers [2], and Dallenbach layers [3], to name just a few examples from the applied electromagnetics literature. Moreover, recent advancements in nanotechnology and materials science have led to the emergence of novel absorber materials, such as graphene-based absorbers [4], carbon-nanotube composites [5], and metal-dielectric metamaterials [6]. In addition, the integration of frequency-selective surfaces [7], metasurfaces [8], and photonic crystals [9] has further enhanced the performance of electromagnetic absorbers by offering a higher degree of control with respect to incident polarization, frequency, angle, and other degrees of freedom. Numerous studies have also focused on the optimization of absorber structures through computational approaches

such as genetic algorithms [10], particle-swarm optimization [11], and deep-learning techniques [12] to achieve superior performance and miniaturization. Furthermore, tunable absorbers that can adapt their absorption properties in real time have also been investigated, such as liquid-crystal-based [13], ferrite-based [14], and phase-change-material-based [15] absorbers. These materials have been shown to provide dynamic control of absorption spectra and enable reconfigurable absorption profiles to suit various applications. Despite the considerable progress in the development of electromagnetic absorbers, however, there still exist several challenges that require further investigation. Among these challenges are the demand for broadband absorption, efficient absorption at low frequencies, and thickness reduction without compromising the absorption performance [16].

To understand the challenges associated with electromagnetic absorption, consider a nonmagnetic absorbing slab characterized by thickness  $d$  and complex permittivity  $\epsilon(\lambda)$  (where  $\lambda$  is the free-space wavelength of the impinging wave), backed by a perfectly reflecting metal mirror, as depicted in Fig. 1(a). To quantify the absorption bandwidth of this configuration, one can consider the maximum allowable reflection magnitude  $\Gamma_0$  within a certain frequency or wavelength range of the reflection-coefficient spectrum  $\Gamma(\lambda)$ , as illustrated in Fig. 1(b). Although increasing the absorber thickness  $d$

\*francesco.monticone@cornell.edu

can generally extend the bandwidth, as in the case of long adiabatically tapered absorbers (e.g., standard anechoic panels), many practical applications call for a broader absorption bandwidth while maintaining a small thickness. Consequently, it is crucially important to identify the physically realizable upper limit for the bandwidth, given a specific  $d$  and a desired reflection reduction (hence a desired absorption level). To address this problem, Rozanov [17] used the analytic properties of the reflection-coefficient function, for passive linear time-invariant (LTI) systems, to establish the theoretical upper bound for the integral of  $\ln |\Gamma(\lambda)|$  over the entire wavelength spectrum (similar to the well-known Bode-Fano limit for matching networks [18]) as

$$\left| \int_0^\infty \ln |\Gamma(\lambda)| d\lambda \right| \leq 2\pi^2 \mu_s d, \quad (1)$$

where  $\mu_s$  is the static relative permeability of the absorbing material (in our case,  $\mu_s = 1$ ). Incidentally, we note that reflection and scattering reduction can be obtained through either absorption effects or interference effects (e.g., with an antireflection coating); the Rozanov bound constrains the former approach and the Bode-Fano limit constrains the latter approach. Here we define the integral on the left side of Eq. (1) as the Rozanov integral, denoted by  $I_R$ . To demonstrate the applicability of Eq. (1) for passive LTI systems, in Fig. 1(c)  $I_R$  was analytically calculated and is plotted for an absorbing material with a lossy Drude-type dispersion for a range of plasma frequencies  $\omega_p$ . This example shows that as the parameters of the system are varied, in this case increasing  $\omega_p$ , the Rozanov integral (and therefore the absorbed energy) may increase to a maximum value and then decrease. This maximum value is limited by the right-hand side of Eq. (1)—referred to as the “Rozanov bound”—which represents a theoretical upper limit for  $I_R$  [see Fig. 1(c)]. Notably, this constraint depends solely on the thickness  $d$  of a nonmagnetic absorber, preventing any further enhancements in absorption performance for traditional passive LTI absorbers. To further explore the connection between absorption performance and thickness, Eq. (1) can be transformed into the following inequality by assuming a reflection magnitude  $\Gamma_0$  within a wavelength range  $\Delta\lambda$  and full reflection outside: [17],

$$|\ln \Gamma_0| \Delta\lambda \leq 2\pi^2 \mu_s d. \quad (2)$$

Equation (2) indicates that lowering the acceptable  $\Gamma_0$  (thereby increasing absorption) would lead to a lower bandwidth  $\Delta\lambda$  as expected. As discussed earlier, increasing absorption while maintaining the same bandwidth requires an increase in the absorber thickness, as illustrated in Fig. 1(d). However, many practical applications call for electromagnetic absorbing layers that can provide efficient

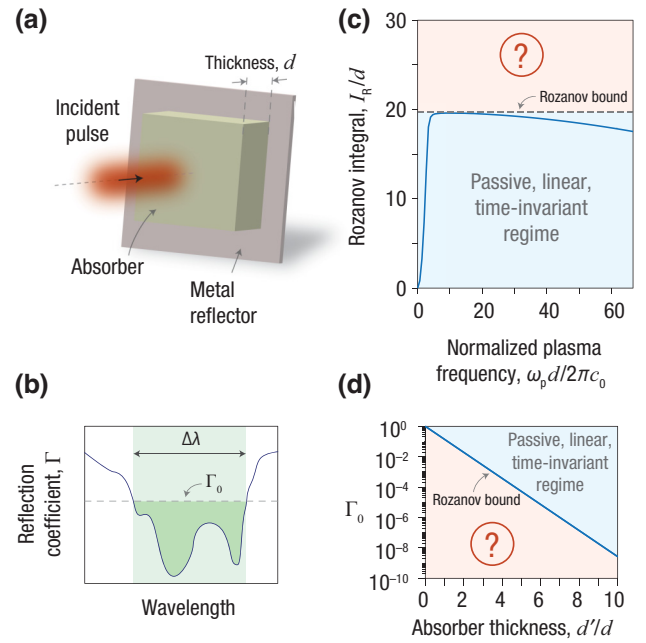


FIG. 1. (a) An electromagnetic pulse impinging on a nonmagnetic absorber with thickness  $d$  backed by a metallic mirror. (b) Illustrative reflection-coefficient spectrum, with the absorption bandwidth determined by the maximum tolerable reflection magnitude ( $\Gamma_0$ ) from the absorber. (c) Practical example demonstrating the constraint on the integral  $I_R$  imposed by the Rozanov bound for passive, linear, and time-invariant absorbers. (d) Implications of the Rozanov bound for electromagnetic absorption, highlighting the typical necessity for increased absorber thickness to improve the absorption performance, for a given bandwidth. The normalized absorption bandwidth in this case is assumed to be  $10d$ . In (c),(d), the considered material has a lossy Drude-type dispersion with a normalized damping coefficient equal to  $\gamma d/2\pi c_0 = 330$ . In (d), the plasma frequency is equal to  $\omega_p d/2\pi c_0 = 6$ , where  $c_0$  is the speed of light in a vacuum.

absorption while maintaining a small thickness and minimal weight, making them suitable for integration into a wide range of devices and systems [19].

A potential approach to break the intrinsic trade-off between bandwidth and thickness and to explore the parameter region not accessible by passive LTI systems [red shaded regions in Figs. 1(c) and 1(d)] is to violate one of the fundamental assumptions of the Rozanov bound: the time-invariant nature of the absorber. While this approach has been explored in the literature, the temporal modulations used were typically limited to “time switching” [20–22], where one or more material properties undergo instantaneous transitions over time. Although this method has significant potential for advancing electromagnetic absorbers beyond the limits of LTI systems, it requires precise synchronization of the switching event, ensuring that the pulse is completely contained within the absorber when it occurs. In addition to the difficulty in attaining precise timing, the need to accommodate a pulse

with a certain spatial width might impose further constraints on the absorber thickness. Moreover, the reduction of reflections within the designated bandwidth often results in a corresponding increase in reflections outside this bandwidth [20,23,24]. This is one of the key mechanisms of such time-varying systems, which reduce reflections within a desired bandwidth not only through absorption but also by redistributing the incident energy beyond the original bandwidth, as also done in phase-modulated lossless screens [23,24]. Finally, we also note that altering material properties instantaneously, or very rapidly, is challenging, especially at optical frequencies [25,26].

Although time switching has been the most-studied approach for challenging theoretical limits in electromagnetics [27], periodic temporal modulations are an intriguing alternative. Periodically modulated electromagnetic and photonic structures (sometimes referred to as photonic time crystals [25,26,28–30]) have recently attracted significant interest due to the wealth of intriguing physical phenomena they unveil [31–33], but their potential for breaking conventional electromagnetic performance bounds has received less attention [34–36]. Similarly to time switching [37,38], periodically modulating a material can alter the frequency spectrum of the probe wave [39–41], which suggests that the trade-off between bandwidth and absorption described above may be modified. However, in contrast to time switching, periodic temporal modulation can lead to parametric processes [42], where the probe wave may experience amplification or absorption within the time-modulated medium [43]. While parametric amplification in periodically modulated systems has attracted considerable attention [29,30,44–48], their absorption aspects have yet to be thoroughly investigated, especially in relation to their implications for overcoming performance limitations in electromagnetics and photonics.

In this study, we explore the properties of periodically temporally-modulated dissipative and dispersive systems, aiming to enhance the absorption performance of thin absorbers beyond the Rozanov bound. Specifically, we examine an approach that combines two distinct absorption mechanisms: material-based and parametric absorption. Our findings reveal that by choosing the proper modulation parameters, one can break the inherent  $\Delta\lambda$ - $d$  trade-off of electromagnetic absorbers and access the parameter space prohibited by the Rozanov bound.

## II. THEORY: WAVES IN A DISSIPATIVE AND DISPERSIVE TIME-MODULATED MEDIUM

In this section, we examine how periodic temporal modulations influence the wave-propagation and absorption properties of an isotropic homogeneous lossy medium with Drude-type dispersive permittivity. Specifically, we consider a medium where the electric polarization density

$\mathbf{P}$  is related to the electric field  $\mathbf{E}$  through

$$\frac{\partial^2 \mathbf{P}}{\partial t^2} + \gamma \frac{\partial \mathbf{P}}{\partial t} = \epsilon_0 \omega_p^2(t) \mathbf{E}, \quad (3)$$

where  $\gamma$  represents the damping coefficient,  $\epsilon_0$  denotes the free-space permittivity, and the plasma frequency  $\omega_p$  is subject to a periodic temporal modulation as

$$\omega_p^2(t) = \omega_{p0}^2 (1 + M \sin(\omega_{\text{mod}} t + \varphi_{\text{mod}})), \quad (4)$$

where  $M$ ,  $\omega_{\text{mod}}$ , and  $\varphi_{\text{mod}}$  are the modulation amplitude, modulation frequency, and modulation phase, respectively, while  $\omega_{p0}$  is the time-invariant plasma frequency in the absence of any temporal modulation. The plasma frequency  $\omega_p$  can be dynamically modulated through several strategies. Among these, the most common method involves altering the free carrier density through carrier injection or depletion via electrical gating in electro-optic structures [49], or through optical carrier injection via light absorption [50]. Another approach involves modifying the average effective mass of the electron sea, which may be achieved by redistributing carriers within a nonparabolic band through intraband absorption, induced by an intense optical pump excitation [25]. In the case of metamaterials operating at microwave frequencies, the effective plasma frequency can be altered through, for example, electrically controlled varactors [51], which may be incorporated in the structure to affect the polarizability and/or density of the unit cells.

As illustrated in Fig. 2(a), an incident optical pulse, with the spatiotemporal profile presented in Fig. 2(c), interacts with the absorber, while the absorber material undergoes a temporal modulation according to Eq. (4). To gain insight into the effect of such a temporal modulation on the incident wave, we start by considering the electromagnetic wave equation in an isotropic homogeneous medium:

$$\frac{\partial^2 \mathbf{D}}{\partial t^2} - \epsilon_0 c_0^2 \nabla^2 \mathbf{E} = 0, \quad (5)$$

where  $\mathbf{D} = \epsilon_0 \mathbf{E} + \mathbf{P}$  is the electric displacement field. Given a spatially homogeneous time modulation, the conservation of the wave vector  $\mathbf{k} = k \hat{\mathbf{z}}$  allows us to express the fields as

$$\Psi = \text{Re}\{\Psi(t)e^{-ikz}\} \mathbf{n}, \quad (6)$$

where  $\mathbf{n}$  is the polarization vector,  $\hat{\mathbf{z}}$  is the unit vector along the propagation direction  $z$ ,  $\Psi = \mathbf{E}, \mathbf{P}$ , or  $\mathbf{D}$ , and  $\Psi(t) = E(t), P(t)$ , or  $D(t)$ . For our analysis, we assume we have a highly dissipative material where  $\gamma$  is very large compared with the probe frequencies in Eq. (3). Consequently, the second-order-differential term on the

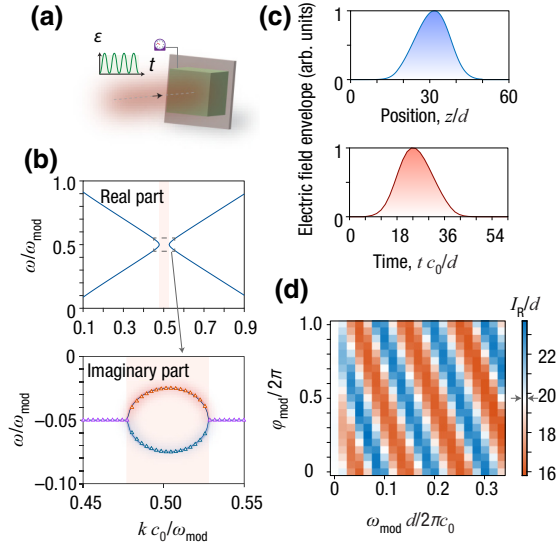


FIG. 2. (a) An incident pulse interacting with an electromagnetic absorber with periodically modulated permittivity. (b) Band structure of the time-modulated material, calculated through the Floquet theorem. The emergence of a momentum band gap in the band structure due to the periodic temporal modulation (upper panel) results in the imaginary part of the eigenfrequency splitting into two distinct values within the gap (lower panel). Triangular markers denote results obtained with the theoretical approach outlined in Sec. II. Material and modulation parameters are as follows:  $\omega_{p0} = 10\omega_{\text{mod}}$ ,  $\gamma = 1000\omega_{\text{mod}}$ , and  $M = 1$ . (c) Spatiotemporal characteristics of the considered incoming pulse. (d) Rozanov-integral  $I_R$  values for a range of modulation parameters. Absorber properties are as follows:  $\omega_{p0}d/2\pi c_0 = 6$ ,  $\gamma d/2\pi c_0 = 330$ , and  $M = 0.4$ . Color-bar arrows in (d) indicate the Rozanov limit.

left-hand side of Eq. (3) can be ignored and Eq. (5) can be rewritten as

$$\frac{d^2 E(t)}{dt^2} + \frac{\omega_p^2(t)}{\gamma} \frac{dE(t)}{dt} + \left( c_0^2 k^2 + \frac{1}{\gamma} \frac{d\omega_p^2(t)}{dt} \right) E(t) = 0. \quad (7)$$

Equation (7) bears resemblance to a harmonic oscillator equation where both the resonance frequency and the damping coefficient are subject to time modulation. To simplify our analysis, we eliminate the first-order-differential “damping” term through the following change of variables:

$$\Theta(t) = e^{\alpha(t)} E(t), \quad \alpha(t) = \frac{1}{2\gamma} \int_0^t \omega_p^2(t') dt'. \quad (8)$$

Equation (7) then becomes

$$\frac{d^2 \Theta(t)}{dt^2} + \Omega(t) \Theta(t) = 0, \quad (9)$$

where, if we use Eq. (4) and ignore terms containing frequencies other than  $\omega_{\text{mod}}$  (as they will lead to off-resonance terms that can be ignored to a first-order approximation in our subsequent derivation),

$$\Omega(t) \approx \omega_0^2 [1 + m_1 \cos(\omega_{\text{mod}} t + \varphi_{\text{mod}}) + m_2 \sin(\omega_{\text{mod}} t + \varphi_{\text{mod}})], \quad (10)$$

$$\omega_0^2 = c_0^2 k^2 - \frac{\omega_{p0}^4}{4\gamma^2} \left( 1 + \frac{M^2}{2} \right), \quad m_1 = \frac{\omega_{p0}^2 \omega_{\text{mod}}}{2\gamma \omega_0^2} M, \quad (11)$$

$$m_2 = -\frac{\omega_{p0}^4}{2\gamma^2 \omega_0^2} M.$$

For  $\omega_{\text{mod}} \approx 2\omega_0$ , the general solution of Eq. (9) can be approximated as [52]

$$\Theta(t) \approx a_1(t) \cos\left(\frac{\omega_{\text{mod}}}{2} t + \frac{\varphi_{\text{mod}}}{2}\right) + a_2(t) \sin\left(\frac{\omega_{\text{mod}}}{2} t + \frac{\varphi_{\text{mod}}}{2}\right), \quad (12)$$

where  $a_1(t)$  and  $a_2(t)$  are slowly varying functions in time compared with the sinusoidal terms. If we insert Eq. (12) into Eq. (9) and ignore the second-order time derivatives of  $a_1(t)$  and  $a_2(t)$  and any terms containing frequencies other than  $\omega_{\text{mod}}/2$  (i.e., using a first-order approximation [52]) we obtain the coupled differential equations

$$\frac{d}{dt} \mathbf{A} = N \mathbf{A}, \quad (13)$$

$$\mathbf{A} = \begin{bmatrix} a_1(t) \\ a_2(t) \end{bmatrix},$$

$$N = \frac{\omega_0^2}{2\omega_{\text{mod}}} \begin{bmatrix} m_2 & -m_1 + 2\Delta\omega \\ -m_1 - 2\Delta\omega & -m_2 \end{bmatrix}, \quad (14)$$

$$\Delta\omega = \frac{4\omega_0^2 - \omega_{\text{mod}}^2}{4\omega_0^2}.$$

The solution for  $\mathbf{A}$  can be found as

$$\mathbf{A} = \kappa_1 \mathbf{V}_1 e^{\nu_1 t} + \kappa_2 \mathbf{V}_2 e^{\nu_2 t}, \quad (15)$$

where  $\kappa_1$  and  $\kappa_2$  are constants that are to be determined from the initial conditions,  $\mathbf{V}_1$  and  $\mathbf{V}_2$  are the eigenvectors of the matrix  $N$ , and  $\nu_1$  and  $\nu_2$  are the corresponding eigenvalues, which can be found as

$$\nu_{1,2} = \pm \frac{\omega_0^2}{2\omega_{\text{mod}}} \sqrt{m_1^2 + m_2^2 - 4\Delta\omega^2}, \quad (16)$$

which shows the condition for having exponentially growing and decaying terms in Eq. (15), namely,  $\Delta\omega^2 < (m_1^2 +$

$m_2^2)/4$ . For  $\Delta\omega = 0$ , the eigenvectors become

$$\mathbf{V}_1 = \begin{bmatrix} m_2 + \sqrt{m_1^2 + m_2^2} \\ -m_1 \end{bmatrix}, \quad \mathbf{V}_2 = \begin{bmatrix} m_1 \\ m_2 + \sqrt{m_1^2 + m_2^2} \end{bmatrix}. \quad (17)$$

A close inspection of Eqs. (12) and (15)–(17) reveals that, for  $\Delta\omega = 0$ , a purely growing  $\Theta(t)$  (i.e.,  $\kappa_1 \neq 0$  and  $\kappa_2 = 0$ ) and a purely decaying  $\Theta(t)$  (i.e.,  $\kappa_1 = 0$  and  $\kappa_2 \neq 0$ ) differ by a modulation phase of  $\varphi_{\text{mod}} = \pi$ . Furthermore, we note from Eq. (8) that the exponential terms for  $E(t)$  become approximately equal to  $\exp\{[\nu_{1,2} - (\omega_{p0}^2/2\gamma)]t\}$ . Generally, in periodically modulated nondispersive nondissipative materials, one of the eigenfrequencies results in exponentially growing fields, while the other corresponds to exponentially decaying fields [42,53]. As the exponentially growing mode dominates, parametric amplification becomes more apparent, whereas observing parametric absorption becomes more challenging [29]. In our case, however, both exponential terms for  $E(t)$  can be designed to exponentially decay with time. One way to achieve this is to ensure that  $(\omega_{p0}^2/\gamma\omega_{\text{mod}})^2 \ll 1$ , so that  $m_2$  can be ignored in comparison with  $m_1$ . In this case, it becomes clear that both exponential terms for  $E(t)$  are exponentially decaying in time as long as  $|M| < 2$  [note that the physically accessible range for  $M$  is  $|M| \leq 1$  according to Eq. (4)]. A more general condition to prevent amplification of the probe wave can be found as  $\omega_{\text{mod}} > \omega_{p0}^2/\sqrt{3}\gamma$  (together with the assumption that  $\gamma$  is much larger than both the probe frequency components and  $\omega_{\text{mod}}$ ), which ensures that the positive eigenvalue in Eq. (16) is smaller than  $\omega_{p0}^2/2\gamma$  for  $\omega_{\text{mod}} = 2\omega_0$ . This is further verified through Bloch-Floquet-theory calculations, which involve expressing the field quantities and time-varying parameters in terms of Bloch-Floquet expansions and solving for the complex eigenfrequency at each wave vector by using the orthogonality of the frequency harmonics [53,54]. The result of this analysis is given in Fig. 2(b), which shows the electromagnetic band structure resulting from the considered dissipative and dispersive periodic temporal modulation. The band structure is characterized by a momentum band gap, in which the imaginary part of the eigenfrequency bifurcates into two separate values, both of which are indeed negative, as independently verified through the theoretical analysis outlined here and the standard Bloch-Floquet method.

In a homogeneous time-varying medium of this type, when a propagating wave has a wave vector falling within the band gap, both modes will generally be excited (i.e., both  $\kappa_1$  and  $\kappa_2$  will become nonzero), one with a higher decay rate and the other with a lower decay rate relative to the time-invariant scenario. Consequently, the overall absorption performance will not be significantly affected compared with the time-invariant case. Although

adjusting the modulation phase in relation to a propagating probe wave can selectively excite the specific eigenmode that favors higher absorption, consistent with theoretical predictions, this generally necessitates a traveling-wave-type spatiotemporal modulation [55]. In contrast, here, the absorbing slab backed by a reflector generates a standing probe wave within the slab, allowing the wave to oscillate either in phase (increased absorption, when  $\kappa_1 = 0$  and  $\kappa_2 \neq 0$ ) or out of phase (reduced absorption, when  $\kappa_1 \neq 0$  and  $\kappa_2 = 0$ ) with the temporal modulation. Note that although our theoretical analysis here is strictly valid only for an unbounded medium, the principle of absorption enhancement via phase-controlled temporal modulation extends to finite-thickness slabs. Indeed, the internal fields of the time-modulated slab are representable through the eigenmodes of the corresponding infinite medium and, therefore, the key features resulting from time modulation in an infinite medium are pertinent to a finite-thickness slab, as was also shown, for instance, in Ref. [29]. We also emphasize that, in addition to the degenerate parametric processes (i.e., coupling between waves at the same frequency via a temporal modulation with modulation frequency approximately twice that of the waves [42]) that lead to waves that grow or decay exponentially with time in a time-modulated infinite medium, a finite slab can also enable nondegenerate parametric processes. Unlike in a time-modulated homogeneous medium, where nondegenerate processes typically do not occur due to a mismatch in wave vectors between the generated harmonic and the bulk propagating mode at the corresponding frequency, a time-modulated finite slab may provide the necessary wave-vector matching through the breaking of spatial translational symmetry. Then the reflected waves originating from fields at frequencies separated by the modulation frequency may destructively interfere when the modulation phase is appropriately adjusted, thereby potentially resulting in further reflection-reduction and enhanced absorption. Consequently, time modulation in a finite slab may not only improve absorption across the frequency bandwidth implied by Eq. (16) but may also extend it to a broader bandwidth where nondegenerate coupling between fields is possible.

The analysis and discussion above provide relevant insights into the problem of a finite periodically-time-modulated lossy slab, consistent with the full-wave numerical simulations reported in the next section. Guided by these theoretical results and predictions, we will show that by carefully selecting the modulation parameters, one can indeed enhance the absorption performance effectively, potentially surpassing the limits of LTI absorbers.

### III. METHODS AND RESULTS: GOING BEYOND THE ROZANOV BOUND

Following the theoretical insight outlined in the previous section, in the following we investigate the

reflection properties of periodically temporally-modulated absorbers and compare them against the Rozanov bound. It is important to note that in the context of time-varying systems, where frequency is not conserved, the reflection coefficient should not generally be represented by  $\Gamma(\omega)$  but should be represented instead by a function  $\Gamma(\omega, \omega')$  that relates the input and output electric fields as  $\mathbf{E}_{\text{out}}(\omega) = \int \Gamma(\omega, \omega') \mathbf{E}_{\text{in}}(\omega') d\omega'$ , as done for other time-varying response functions [43]. Nevertheless, for a specific incoming signal, one may also define an equivalent input-dependent reflection coefficient  $\Gamma_{\text{eq}}(\omega)$  via the relation  $\mathbf{E}_{\text{out}}(\omega) = \Gamma_{\text{eq}}(\omega) \mathbf{E}_{\text{in}}(\omega)$  to compute  $I_R$  within the frequency range of the incident pulse. Note that because of the frequency-nonconserving nature of the time-modulated system, this equivalent reflection coefficient will be valid only for the considered input field with its specific temporal/spectral profile, and will be useful only for the case of sufficiently broadband signals for which the generated reflected fields at frequencies beyond the bandwidth of the original signal would be negligible. The case of generic and narrowband incident pulses is treated differently in the following, resulting however in similar results in terms of absorption enhancement. Thus, we consider here an incoming pulse with an ultrawide bandwidth, corresponding to a normalized wavelength range from  $\lambda/d = 0.02$  to  $\lambda/d = 1000$ , and we numerically compute  $I_R$  over this broad wavelength range to evaluate the absorption performance of the system (we assume the integrand of  $I_R$  is zero outside this range). It should also be noted that for a generic time-varying system the magnitude of the reflection coefficient may be larger than unity at certain wavelengths, due to parametric amplification and/or harmonic generation, which would imply a reduction of  $I_R$ . In contrast, our approach based on parametrically enhanced absorption is expected to increase  $I_R$ , potentially beyond the Rozanov bound [the right-hand side of Eq. (1)]. To demonstrate this opportunity for enhanced absorption performance, the Rozanov integral for the input given in Fig. 2(c) was numerically calculated with use of the finite-difference time-domain method [56]. The spatial and time resolutions were set to  $0.033d$  and  $0.006476d/c_0$ , respectively, to ensure numerical stability and convergence of the solution for a range of modulation parameters, as shown in Fig. 2(d). It is evident that for  $\omega_{\text{mod}} = 0$  (i.e., time-invariant case)  $I_R$  consistently remains below the Rozanov bound. However, when the modulation frequency  $\omega_{\text{mod}}$  takes on nonzero values, the Rozanov integral can exceed the Rozanov bound for certain modulation parameters. It is important to note that the frequency spectrum of the input field is sufficiently broad, allowing each of the considered  $\omega_{\text{mod}}$  to enable the parametric processes that enhance absorption (which occurs when the modulation frequency is twice the signal frequency). Moreover, as expected from our theoretical analysis, the absorption performance depends on the modulation phase  $\varphi_{\text{mod}}$ ,

indicating an optimal  $\varphi_{\text{mod}}$  for each modulation frequency, for which the eigenmode with higher absorption can be selectively excited. It is also worth mentioning that the spatial width of the impinging pulse [see Fig. 2(c)] is significantly larger than the thickness ( $d$ ) of the absorber. This situation would not be suitable for time-switched systems [20,21], where the switching needs to occur when the pulse is entirely contained within the system.

To further investigate the effect of the temporal modulation on the absorption characteristics, Fig. 3(a) shows the calculated  $I_R$  for the full range of modulation amplitudes  $M$  for the same broadband incident pulse. Remarkably, Fig. 3(a) shows that in this scenario, even for small modulation amplitudes ( $M \sim 0.05$ ), it is possible to surpass the Rozanov bound. Interestingly, the  $I_R$ - $M$  curve presents a peak, after which an increase in  $M$  leads to a decrease in the integral value of  $I_R$ . We ascribe this behavior to the intricate interplay of harmonic redistribution effects and parametric processes in this time-varying medium. Although parametric processes could reduce reflection at specific wavelengths, the harmonic redistribution due to the temporal modulation may increase the reflection coefficient at adjacent wavelengths. Consequently, this may establish an optimal point where  $I_R$  reaches its maximum value. To examine more closely the absorption characteristics of the time-modulated system, Fig. 3(b) shows the superimposed reflection coefficient for the time-invariant ( $M = 0$ ) and time-modulated ( $M = 0.96$ ) cases. It is clear that when the absorber is temporally modulated the reflection diminishes considerably across an extensive wavelength spectrum, ranging from  $\lambda/d = 0.5$  to  $\lambda/d = 15$ , while the reflection experiences an increase at wavelengths adjacent to this range. Overall,  $I_R$  increases beyond the Rozanov bound, given that it is primarily influenced by the wavelength range where the reflection experiences a strong reduction.

Moreover, to further improve the absorption performance for a broadband impinging pulse, the modulation frequency can be made multiharmonic, i.e.,

$$\omega_p^2(t) = \omega_{p0}^2 \left( 1 + M \sum_n \sin(\omega_{\text{mod}_n} t + \varphi_{\text{mod}_n}) \right), \quad (18)$$

which allows optimization of absorption for multiple frequency ranges within the signal bandwidth. As demonstrated in Figs. 3(c) and 3(d), this method has the potential advantage of requiring smaller modulation amplitudes (around 0.32) for each of the three modulation frequency components to achieve absorption performance comparable to the case of a single-frequency modulation, owing to the possibility of combining reflection reductions across multiple frequency ranges. It is also worth noting that the reflections occurring outside the enhanced absorption window do not experience a significant increase, as is the case with a single-frequency modulation [compare Figs.

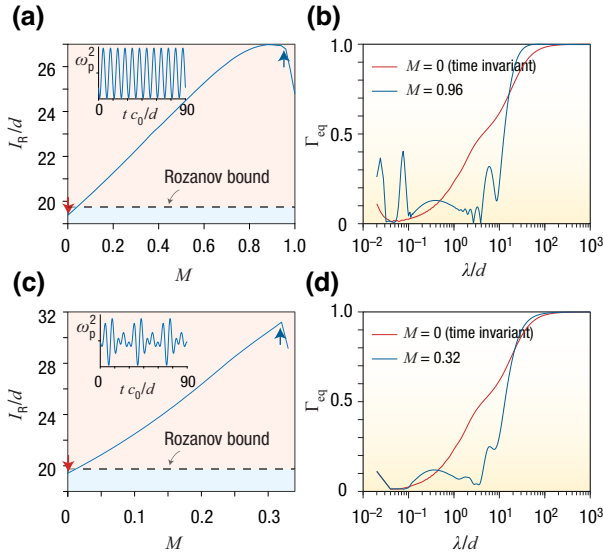


FIG. 3. (a) Computed Rozanov integral  $I_R$  as a function of the modulation amplitude. (b) Superimposed reflection-coefficient spectra for  $M = 0$  (time invariant), and  $M = 0.96$  [denoted with red and blue arrows, respectively, in (a)]. Absorber properties are the same as for Fig. 2, with  $\varphi_{\text{mod}}/\pi = 0.60$  and  $\omega_{\text{mod}}d/2\pi c_0 = 0.133$ . (c),(d) Same as (a) and (b) but with a multiharmonic modulation function with modulation frequencies  $\omega_{\text{mod}_1}d/2\pi c_0 = 0.100$ ,  $\omega_{\text{mod}_2}d/2\pi c_0 = 0.133$ , and  $\omega_{\text{mod}_3}d/2\pi c_0 = 0.166$ , modulation phases  $\varphi_{\text{mod}_1}/2\pi = 0.90$ ,  $\varphi_{\text{mod}_2}/2\pi = 0.60$ , and  $\varphi_{\text{mod}_3}/2\pi = 0.25$ , and the same modulation amplitude  $M$  for each individual modulation harmonic. The upper-left insets in (a),(b) show the periodic temporal modulations given by Eqs. (4) and (18), respectively.

3(b) and 3(d)]. This primarily occurs because the lower amplitudes of the individual modulation components, each with different frequency, are not sufficient to induce strong harmonic generations at these wavelengths.

While the previous analysis focused on an ultrabroadband input field, we also explored the time-varying absorber response for a field with relatively narrow bandwidth. In this situation,  $I_R$  may not serve as a reliable measure of the absorption performance, as the equivalent reflection coefficient, defined as above, would take extremely large values or even become infinite beyond the input-pulse bandwidth. Thus, following an approach similar to that in Ref. [21], a figure of merit denoted as “absorption efficiency” is defined to evaluate the absorption performance, and compare it against the Rozanov bound, over the entire electromagnetic spectrum:

$$\eta_{\text{abs}} = 1 - \frac{\int_{-\infty}^{\infty} |E_{\text{ref}}(\lambda)|^2 d\lambda}{\int_{-\infty}^{\infty} |E_{\text{inc}}(\lambda)|^2 d\lambda}, \quad (19)$$

where  $E_{\text{ref}}$  and  $E_{\text{inc}}$  are, respectively, the reflected-electric-field spectrum and the incident-electric-field spectrum. Note that this formulation differs slightly from that in

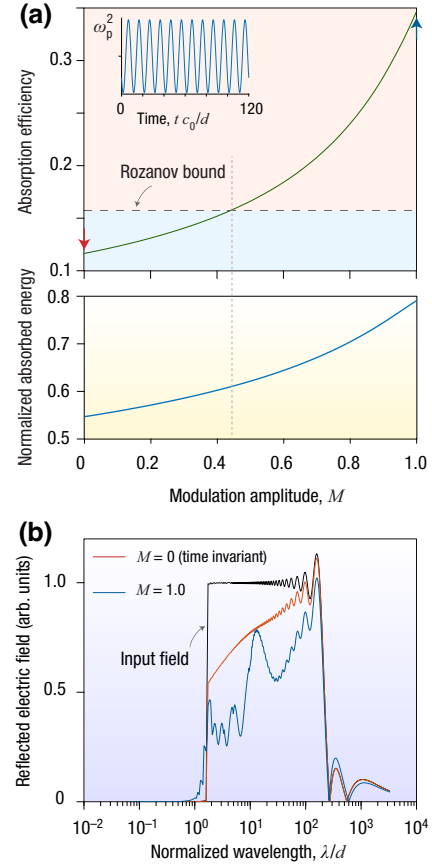


FIG. 4. (a) Calculated absorption efficiency (upper panel), as defined in the main text, and absorbed energy (lower panel), normalized to incident energy, both plotted as a function of the modulation amplitude. The upper-left inset shows the periodic temporal modulation. (b) Superimposed spectra of the reflected electric field for  $M = 0$  (time invariant) and  $M = 1.0$  [denoted with red and blue arrows, respectively, in (a)]. Absorber properties are as follows:  $\omega_{p0}d/2\pi c_0 = 5.5$ ,  $\gamma d/2\pi c_0 = 100$ ,  $\varphi_{\text{mod}}/\pi = 0.45$ , and  $\omega_{\text{mod}}d/2\pi c_0 = 0.1$ .

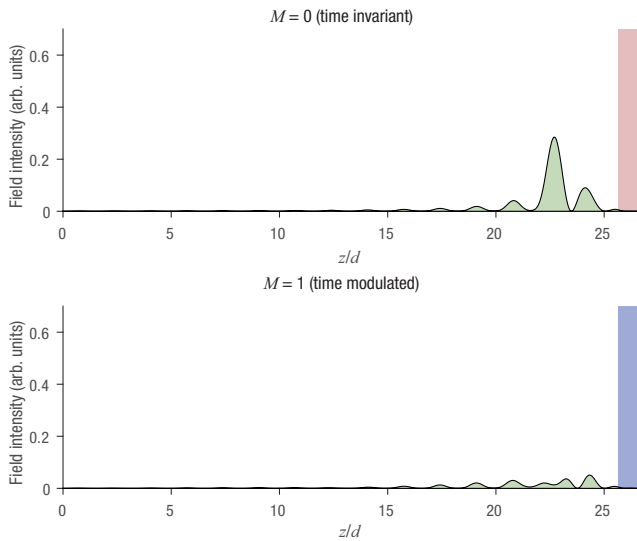
Ref. [21], where the integration is done over frequency rather than wavelength. This choice is to ensure a direct comparison with the Rozanov bound, which is derived by an integration in the complex-wavelength domain. According to this definition of the figure of merit, the corresponding Rozanov bound for the LTI case can be written as

$$\eta_{\text{abs,R}} = 1 - \frac{\int_{-\infty}^{\infty} |\Gamma_0 E_{\text{inc}}(\lambda)|^2 d\lambda}{\int_{-\infty}^{\infty} |E_{\text{inc}}(\lambda)|^2 d\lambda}, \quad (20)$$

where  $\Gamma_0$  assumes the lowest value it is allowed to take for the given bandwidth  $\Delta\lambda$ , according to Eq. (2), i.e.,

$$\Gamma_0 = e^{-2\pi^2 d/\Delta\lambda} \quad (21)$$

within the considered wavelength range and  $\Gamma_0 = 1$  outside this range. Note that for an accurate comparison with



**VIDEO 1.** Time-domain animation of an incident pulse interacting with a time-varying absorber (lower panel) and its time-invariant counterpart (upper panel).

the Rozanov bound, the incident pulse should exhibit a sufficiently-well-defined bandwidth, while having minimal energy outside this range, as in the case in Fig. 4. As an example, the absorption efficiency for a signal with a wavelength bandwidth ranging from  $\lambda/d = 1.66$  to  $\lambda/d = 200$  was calculated for a range of modulation parameters [see Fig. 4(a)]. Similarly to the trend observed in Fig. 3(a), these results clearly show that the absorption performance improves in the time-varying case and can surpass the Rozanov bound by a significant amount. To supplement this result, the lower panel in Fig. 4(a) directly shows the absorbed energy (normalized to the incident energy) with respect to the modulation amplitude, confirming an increase in absorption compared with the time-invariant scenario. To further clarify the reflection response of the time-modulated absorber, Fig. 4(b) displays the superimposed reflection spectrum for the time-invariant and time-varying cases. When the material is temporally modulated, the reflected field is indeed reduced almost everywhere within the incident pulse bandwidth. Although extra harmonics are generated at shorter wavelengths beyond this bandwidth [as can be observed in Fig. 4(b)], the strong reduction of in-band reflection results in an overall increase of absorption efficiency that allows the Rozanov bound to be surpassed. It should also be emphasized that the amount of reflection reduction varies across the signal bandwidth, with some spectral regions experiencing minimal decrease with respect to the time-invariant case. We attribute this variability to the interaction between material-loss-induced and parametric-process-induced absorption and the spectral redistribution caused by the periodic modulation. We also note that the absorption efficiency increases monotonically with the modulation amplitude in this case, which we

attribute to the fact that the amplitude of the generated harmonics outside the original bandwidth is not large enough to saturate this increasing trend [unlike, for example, the case in Figs. 3(a) and 3(b)]. Finally, in Video 1, we provide a time-domain animation that shows the incident pulse interacting with the time-varying absorber and the resulting reflection. For comparison, the animation also shows the corresponding time-invariant scenario, further confirming the broadband reduction in reflection, and enhancement in absorption, due to time modulation.

#### IV. SUMMARY

In conclusion, we have examined the relatively unexplored absorption aspects of periodically temporally modulated lossy materials, focusing on their implications to surpass the electromagnetic absorption limits of linear time-invariant systems. Our findings—in terms of two different figures of merit (Rozanov integral of the reflection coefficient, and absorption efficiency)—consistently show that by selecting appropriate modulation parameters, one can drastically enhance the absorption performance of the system compared with that of its time-invariant counterpart and even surpass the Rozanov bound for electromagnetic absorption, fundamentally breaking the trade-off between thickness, bandwidth, and reflection reduction. In contrast to time-switched mechanisms [20,21], our method does not require exact timing to guarantee that the pulse is entirely contained within the absorber; instead, the considered periodic modulation is continuously applied as the pulse enters the absorbing medium. As a result, our platform automatically addresses the issue of impedance mismatch at the entrance interface between the absorber and free space, whereas in time-switched platforms the impedance mismatch problem is typically resolved through additional optimizations. Moreover, our approach ensures that the absorber thickness is independent of the pulse spatial width, whereas in time-switched platforms the minimum slab thickness is typically limited by the pulse width. It is also worth mentioning that since both eigenmodes in the momentum band gap of the periodically modulated structure have a decaying nature, due to the high intrinsic losses of the considered material, the system is free from any instabilities, namely, unbounded temporal oscillations.

Finally, while the generalization of the Rozanov bound to time-varying systems remains a very interesting open question that will be the subject of future research, we can make the following general observations about what changes in the non-LTI case. First, a time-varying medium can alter the frequency content and bandwidth of the propagating signal [27], thereby relaxing constraints set by the Rozanov bound based on the original bandwidth. Any generalization of this bound to time-varying systems will need to account for these effects. More fundamentally, as mentioned in Sec. III, while reflected fields are well-defined



in both LTI and linear time-varying cases, the reflection coefficient needs to be generalized to account for coupling between different frequencies (similarly to the transfer functions of nonlinear optical processes [57]). Moreover, in stable LTI systems, causality of the reflection coefficient implies its analyticity in one of the complex-frequency or complex-wavelength half-planes, upon which the Rozanov bound is contingent. This is no longer generally guaranteed in non-LTI systems, making the bound no longer applicable. Indeed, any generalized reflection coefficient for these systems may have very different analytic properties. This is indeed the case for nonlinear optical media (and, therefore, time-varying systems realized through nonlinear processes), where causal transfer functions may not be strictly analytic or holomorphic, but could be meromorphic [57].

These observations, and our findings presented in the previous sections, suggest that judiciously designed non-LTI systems have great potential to overcome conventional physical limits that were originally derived for LTI systems. Along this line, we hope that our work may provide a new route for the design of advanced electromagnetic absorbers that can surpass such bounds.

### ACKNOWLEDGMENTS

The authors acknowledge support from the Air Force Office of Scientific Research with Grant No. FA9550-22-1-0204 and the Office of Naval Research with Grant No. N00014-22-1-2486.

- 
- [1] W. W. Salisbury, Absorbent body for electromagnetic waves (1952), US Patent 2,599,944.
  - [2] E. Knott and K. Langseth, Performance degradation of Jaumann absorbers due to curvature, *IEEE Trans. Antennas Propag.* **28**, 137 (1980).
  - [3] W. Dallenbach and W. Kleinstuber, Reflection and absorption of decimeter-waves by plane dielectric layers, *Hochfreq. u. Elektroak* **51**, 152 (1938).
  - [4] M. Amin, M. Farhat, and H. Bağcı, An ultra-broadband multilayered graphene absorber, *Opt. Express* **21**, 29938 (2013).
  - [5] A. Saib, L. Bednarz, R. Daussin, C. Bailly, X. Lou, J.-M. Thomassin, C. Pagnoulle, C. Detrembleur, R. Jérôme, and I. Huynen, Carbon nanotube composites for broadband microwave absorbing materials, *IEEE Trans. Microw. Theory Tech.* **54**, 2745 (2006).
  - [6] G. Dayal and S. A. Ramakrishna, Design of multi-band metamaterial perfect absorbers with stacked metal-dielectric disks, *J. Opt.* **15**, 055106 (2013).
  - [7] L. Sun, H. Cheng, Y. Zhou, and J. Wang, Broadband metamaterial absorber based on coupling resistive frequency selective surface, *Opt. Express* **20**, 4675 (2012).
  - [8] H. Wakatsuchi, S. Kim, J. J. Rushton, and D. F. Sievenpiper, Waveform-dependent absorbing metasurfaces, *Phys. Rev. Lett.* **111**, 245501 (2013).
  - [9] Y. Nam, Y. X. Yeng, A. Lenert, P. Bermel, I. Celanovic, M. Soljačić, and E. N. Wang, Solar thermophotovoltaic energy conversion systems with two-dimensional tantalum photonic crystal absorbers and emitters, *Solar Energy Mater. Solar Cells* **122**, 287 (2014).
  - [10] E. Michielssen, J.-M. Sajer, S. Ranjithan, and R. Mittra, Design of lightweight, broad-band microwave absorbers using genetic algorithms, *IEEE Trans. Microwave Theory Tech.* **41**, 1024 (1993).
  - [11] S. Cui and D. S. Weile, Application of a parallel particle swarm optimization scheme to the design of electromagnetic absorbers, *IEEE Trans. Antennas Propag.* **53**, 3616 (2005).
  - [12] J. Hou, H. Lin, W. Xu, Y. Tian, Y. Wang, X. Shi, F. Deng, and L. Chen, Customized inverse design of metamaterial absorber based on target-driven deep learning method, *IEEE Access* **8**, 211849 (2020).
  - [13] D. Shrekenhamer, W.-C. Chen, and W. J. Padilla, Liquid crystal tunable metamaterial absorber, *Phys. Rev. Lett.* **110**, 177403 (2013).
  - [14] M. Lei, N. Feng, Q. Wang, Y. Hao, S. Huang, and K. Bi, Magnetically tunable metamaterial perfect absorber, *J. Appl. Phys.* **119**, 244504 (2016).
  - [15] M. A. Kats, D. Sharma, J. Lin, P. Genevet, R. Blanchard, Z. Yang, M. M. Qazilbash, D. Basov, S. Ramanathan, and F. Capasso, Ultra-thin perfect absorber employing a tunable phase change material, *Appl. Phys. Lett.* **101**, 221101 (2012).
  - [16] X. Zeng, X. Cheng, R. Yu, and G. D. Stucky, Electromagnetic microwave absorption theory and recent achievements in microwave absorbers, *Carbon* **168**, 606 (2020).
  - [17] K. N. Rozanov, Ultimate thickness to bandwidth ratio of radar absorbers, *IEEE Trans. Antennas Propag.* **48**, 1230 (2000).
  - [18] D. M. Pozar, *Microwave Engineering*, 4th ed. (John Wiley & Sons, Hoboken, NJ, USA, 2011).
  - [19] Y. Ra'idi, C. R. Simovski, and S. A. Tretyakov, Thin perfect absorbers for electromagnetic waves: Theory, design, and realizations, *Phys. Rev. Appl.* **3**, 037001 (2015).
  - [20] H. Li and A. Alù, Temporal switching to extend the bandwidth of thin absorbers, *Optica* **8**, 24 (2021).
  - [21] C. Firestein, A. Shlivinski, and Y. Hadad, Absorption and scattering by a temporally switched lossy layer: Going beyond the Rozanov bound, *Phys. Rev. Appl.* **17**, 014017 (2022).
  - [22] X. Yang, E. Wen, and D. F. Sievenpiper, Broadband time-modulated absorber beyond the Bode-Fano limit for short pulses by energy trapping, *Phys. Rev. Appl.* **17**, 044003 (2022).
  - [23] A. Tennant, Reflection properties of a phase modulating planar screen, *Electron. Lett.* **33**, 1768 (1997).
  - [24] B. Chambers and A. Tennant, A smart radar absorber based on the phase-switched screen, *IEEE Trans. Antennas Propag.* **53**, 394 (2005).
  - [25] S. Saha, O. Segal, C. Fruhling, E. Lustig, M. Segev, A. Boltasseva, and V. M. Shalaev, Photonic time crystals: A materials perspective, *Opt. Express* **31**, 8267 (2023).
  - [26] Z. Hayran, J. B. Khurgin, and F. Monticone,  $\hbar\omega$  versus  $\hbar k$ : Dispersion and energy constraints on time-varying photonic

- materials and time crystals, *Opt. Mater. Express* **12**, 3904 (2022).
- [27] Z. Hayran and F. Monticone, Using time-varying systems to challenge fundamental limitations in electromagnetics: Overview and summary of applications, *IEEE Antennas Propag. Mag.* **65**, 29 (2023).
- [28] A. Dikopoltsev, Y. Sharabi, M. Lyubarov, Y. Lumer, S. Tseskes, E. Lustig, I. Kaminer, and M. Segev, Light emission by free electrons in photonic time-crystals, *Proc. Natl. Acad. Sci.* **119**, e2119705119 (2022).
- [29] X. Wang, M. S. Mirmoosa, V. S. Asadchy, C. Rockstuhl, S. Fan, and S. A. Tretyakov, Metasurface-based realization of photonic time crystals, *Sci. Adv.* **9**, eadg7541 (2023).
- [30] M. Lyubarov, Y. Lumer, A. Dikopoltsev, E. Lustig, Y. Sharabi, and M. Segev, Amplified emission and lasing in photonic time crystals, *Science* **377**, 425 (2022).
- [31] Y. Hadad, J. C. Soric, and A. Alu, Breaking temporal symmetries for emission and absorption, *Proc. Natl. Acad. Sci.* **113**, 3471 (2016).
- [32] P. A. Huidobro, E. Galiffi, S. Guenneau, R. V. Craster, and J. B. Pendry, Fresnel drag in space-time-modulated metamaterials, *Proc. Natl. Acad. Sci.* **116**, 24943 (2019).
- [33] S. Yin, E. Galiffi, and A. Alù, Floquet metamaterials, *ELight* **2**, 1 (2022).
- [34] H. Li, A. Mekawy, and A. Alù, Beyond Chu's limit with Floquet impedance matching, *Phys. Rev. Lett.* **123**, 164102 (2019).
- [35] S. Suwunnarat, D. Halpern, H. Li, B. Shapiro, and T. Kottos, Dynamically modulated perfect absorbers, *Phys. Rev. A* **99**, 013834 (2019).
- [36] M. Mostafa, A. Díaz-Rubio, M. Mirmoosa, and S. Tretyakov, Coherently time-varying metasurfaces, *Phys. Rev. Appl.* **17**, 064048 (2022).
- [37] H. Moussa, G. Xu, S. Yin, E. Galiffi, Y. Ra'di, and A. Alù, Observation of temporal reflection and broadband frequency translation at photonic time interfaces, *Nat. Phys.* **19**, 863 (2023).
- [38] A. Shlivinski and Y. Hadad, Beyond the Bode-Fano bound: Wideband impedance matching for short pulses using temporal switching of transmission-line parameters, *Phys. Rev. Lett.* **121**, 204301 (2018).
- [39] J. R. Zurita-Sánchez and P. Halevi, Resonances in the optical response of a slab with time-periodic dielectric function  $\varepsilon(t)$ , *Phys. Rev. A* **81**, 053834 (2010).
- [40] T. T. Koutserimpas and R. Fleury, Electromagnetic waves in a time periodic medium with step-varying refractive index, *IEEE Trans. Antennas Propag.* **66**, 5300 (2018).
- [41] E. Galiffi, R. Tirole, S. Yin, H. Li, S. Vezzoli, P. A. Huidobro, M. G. Silveirinha, R. Sapienza, A. Alù, and J. Pendry, Photonics of time-varying media, *Adv. Photonics* **4**, 014002 (2022).
- [42] S. Lee, J. Park, H. Cho, Y. Wang, B. Kim, C. Daraio, and B. Min, Parametric oscillation of electromagnetic waves in momentum band gaps of a spatiotemporal crystal, *Photonics Res.* **9**, 142 (2021).
- [43] J. Sloan, N. Rivera, J. D. Joannopoulos, and M. Soljačić, Optical properties of dispersive time-dependent materials, *ACS Photonics* **11**, 950 (2024).
- [44] J. Park, H. C. Park, K. Lee, J. Shin, J.-W. Ryu, W. Jeon, N. Park, and B. Min, Comment on "Amplified emission and lasing in photonic time crystals", Preprint [ArXiv:2211.14832](https://arxiv.org/abs/2211.14832) (2022).
- [45] J. Gaxiola-Luna and P. Halevi, Growing fields in a temporal photonic (time) crystal with a square profile of the permittivity  $\varepsilon(t)$ , *Appl. Phys. Lett.* **122**, 011702 (2023).
- [46] V. Asadchy, A. Lampranidis, G. Ptitcyn, M. Albooyeh, T. Karamanos, R. Alaee, S. Tretyakov, C. Rockstuhl, S. Fan, *et al.*, Parametric Mie resonances and directional amplification in time-modulated scatterers, *Phys. Rev. Appl.* **18**, 054065 (2022).
- [47] T. T. Koutserimpas and R. Fleury, Nonreciprocal gain in non-Hermitian time-Floquet systems, *Phys. Rev. Lett.* **120**, 087401 (2018).
- [48] V. Pacheco-Peña, Y. Kiasat, D. M. Solís, B. Edwards, and N. Engheta, Holding and amplifying electromagnetic waves with temporal non-Foster metastructures, Preprint [ArXiv:2304.03861](https://arxiv.org/abs/2304.03861) (2023).
- [49] E. Feigenbaum, K. Diest, and H. A. Atwater, Unity-order index change in transparent conducting oxides at visible frequencies, *Nano Lett.* **10**, 2111 (2010).
- [50] S. Leonard, H. Van Driel, J. Schilling, and R. Wehrspohn, Ultrafast band-edge tuning of a two-dimensional silicon photonic crystal via free-carrier injection, *Phys. Rev. B* **66**, 161102 (2002).
- [51] I. Gil, J. Bonache, J. Garcia-Garcia, and F. Martin, Tunable metamaterial transmission lines based on varactor-loaded split-ring resonators, *IEEE Trans. Microw. Theory Tech.* **54**, 2665 (2006).
- [52] L. D. Landau and E. M. Lifshitz, *Mechanics: Course of Theoretical Physics*, 3rd ed. (Butterworth-Heinemann, Oxford, UK, 1976), Vol. 1, §27. Parametric resonance, p. 80.
- [53] N. Chamanara, Z.-L. Deck-Léger, C. Caloz, and D. Kalluri, Unusual electromagnetic modes in space-time-modulated dispersion-engineered media, *Phys. Rev. A* **97**, 063829 (2018).
- [54] S. Taravati and A. A. Kishk, Space-time modulation: Principles and applications, *IEEE Microw. Mag.* **21**, 30 (2020).
- [55] E. Galiffi, P. Huidobro, and J. B. Pendry, Broadband nonreciprocal amplification in luminal metamaterials, *Phys. Rev. Lett.* **123**, 206101 (2019).
- [56] Ansys Lumerical FDTD Solutions 2022, <https://www.lumerical.com/products/fdtd/> (2022).
- [57] V. Lucarini, K. E. Peiponen, J. J. Saarinen, and E. M. Vartiainen, in *Kramers-Kronig Relations in Optical Materials Research* (Springer Science & Business Media, Berlin, Germany, 2005), Chapter 9. Modified Kramers-Kronig Relations in Nonlinear Optics.